Electron-stimulated desorption of positive ions from physisorbed monolayers of H_2, HD, and D_2 on graphite and D_2 on Kr-plated graphite

S. C. Fain, Jr.,* Bin Xia, and Joe Peidle†
Department of Physics, University of Washington, Seattle, Washington 98195
(Received 25 April 1994; revised manuscript received 5 July 1994)

Angular distribution, time-of-flight, retarding field, and effective positive-ion cross-section measurements are presented for positive ions produced by electron-stimulated desorption from physisorbed monolayers of H_2, HD, and D_2 on graphite and from D_2 on Kr-plated graphite. The electron energy was 60–63 eV, except as noted. The angular distributions are isotropic in the range of 140°–170° from the forward direction of the normally incident electron beam. Diatomic and triatomic ions are each less than 1% of the positive ions detected; the rest are monatomic ions (H^+ and/or D^+). The proportion of higher energy H^+ ions from H_2 increases as the electron energy is raised above 30 eV, the threshold for dissociative ionization from the $^2\Sigma_u^+(2p\sigma)$ antibonding state of the diatomic positive ion. The proportion of low-energy D^+ ions is larger for D_2 on Kr-plated graphite than for D_2 on bare graphite. Retarding field measurements were fit assuming one or two Gaussian components of monatomic-ion kinetic-energy distributions; the most probable monatomic-ion kinetic energies (without contact-potential corrections) were 5.7 eV for H^+ from H_2; 5.4 eV for D^+ from D_2; 7.9 eV for H^+ from HD; 2.6 eV for D^+ from HD; and 1.2 eV for D^+ from D_2 on Kr-plated graphite. The ratio of the number of H^+ ions to the number of D^+ ions from HD decreases from 3.1 to 2.9 as the coverage is increased from commensurate to incommensurate. The effective positive-ion cross sections are estimated within a factor of 2 to be 1×10^{-5}, 3×10^{-6}, and 1×10^{-6} nm^2 for H_2, HD, and D_2.

I. INTRODUCTION

H_2, HD, and D_2 molecules adsorb layer by layer without dissociation on the graphite basal plane at $T<20$ K.[1] A number of interesting structures and phase transitions occur for multilayers and for incommensurate monolayers.[1–3] At low coverages and $T<10$ K all three isotopes form two-dimensional (2D) islands of a commensurate $\sqrt{3}\times\sqrt{3}R30°$ structure surrounded by low-density 2D gas.[1] One result of the weak interactions of the molecules with the substrate and other adsorbed molecules is the lack of a strongly preferred direction of the molecular axes in the commensurate structure for $T>1$ K. Theoretical calculations indicate that the ground state for D_2 (H_2) molecules in the commensurate phase has less than 3% (1%) admixture of quantum states with nonzero rotational state angular momentum J.[4] Electron-energy-loss spectroscopy measurements from H_2 show that the energy of the $J=0$ to $J=2$ rotational transition is the same as for the gas phase within experimental uncertainties.[5] Ordering of the molecular axes in the commensurate phase has been observed for metastable $J=1$ ortho-H_2 only for $T<0.6$ K.[6] Another result of the weak lateral interactions in the commensurate phase is a phonon spectrum with only small dispersion, especially for D_2.[7]

For many chemisorbed molecules, the study of positive ions produced by electron stimulated desorption (ESD) has given valuable information about the bonding geometry and energetics.[8] Due to the weak interactions of the physisorbed H_2, HD, and D_2 molecules mentioned above, one might expect the angle, mass, and kinetic-energy distributions of H^+ and D^+ from monolayers to be similar to those observed in gas phase dissociative ionization by electrons of similar energies.

Several processes leading to monatomic ions for electrons of energy between 30–60 eV incident on H_2 in the gas phase have been identified in the literature.[9–11]

(1) Direct ionization of the neutral molecule to a singly ionized excited state which can subsequently dissociate,[9,12]

$$e^- + H_2 \rightarrow 2e^- + H_2^{+*} \rightarrow 2e^- + H + H^+ .$$

The $^2\Sigma_g^+(1s\sigma)$ bonding state for electron energies greater than 18 eV leads to near-zero-energy protons; the $^2\Sigma_u^+(2p\sigma)$ antibonding state for electron energies greater than 28 eV leads to protons with energies of 5 eV or more.

(2) Excitation to doubly excited repulsive states of the neutral molecule which autoionize into the vibrational continuum of the $^2\Sigma_g^+(1s\sigma)$,[11,13–15]

$$e^- + H_2 \rightarrow e^- + H_2^{**} \rightarrow 2e^- + H_2^{+*} \rightarrow 2e^- + H + H^+ .$$

At least five such autoionizing states have been observed for H_2 with electron threshold energies from 22 to 28 eV; the protons produced have energies less than 6 eV.[11]

(3) Ion pair production via various possible intermediate states,[9,11,16]

$$e^- + H_2 \rightarrow e^- + H^- + H^+ .$$

This process has an electron threshold of 17 eV.[9]

(4) Double ionization of the neutral molecule,[17]

$$e^- + H_2 \rightarrow 3e^- + H^+ + H^+ .$$

This process has an electron threshold of 46 eV.

In the gas phase at 60 eV, the cross sections for processes 3 and 4 are estimated to be at least a factor of 100 smaller than the processes 1 and 2 which together[18] have a cross section of about 1×10^{-3} nm^2. The contribution of process 2 to the total production of H^+ has recently been estimated to be $\geq 30\%$ ($\geq 40\%$) at 40 eV (100 eV) electron energy.[15] In the gas phase the predominant product of ionization is positive diatomic ions,[18]

$$e^- + H_2 \rightarrow e^- + H_2^+ ,$$

with a cross section of 1×10^{-2} nm^2 at 60 eV.

Measurements of positive-ion ESD from physisorbed D_2 on Pd(111) with a chemisorbed D monolayer[19] found monatomic ions to be the largest desorbed product from a physisorbed monolayer; diatomic and triatomic ions became a larger fraction of the product for multilayers. The low-velocity positive ions generated in a monolayer are much more likely to undergo neutralization by the substrate electrons, leading to the low numbers of diatomic relative to monatomic ions.[8,20] In addition, the attractive force related to image charge effects[8,21] will prevent the lowest-energy ions from escaping from the surface. The triatomic ions seen for multilayers can arise from collisions of monatomic ions with diatomic neutral molecules,[19,22]

$$H^+ + 2H_2 \rightarrow H_2 + H_3^+ .$$

The study of physisorbed D_2 on Pd(111) with a chemisorbed D monolayer focused on the desorption from multilayers of D_n^+ clusters comprised of odd numbers of atoms.[19] In addition the $^2\Sigma_u^+(2p\sigma)$ antibonding state was identified as the primary source of energetic D^+ ions.[19] Quantitative measurements of the ion energy distributions and effective cross sections were not made.

In the present paper, we investigate the positive-ion angle, mass, and kinetic-energy distribution produced by ESD of H_2, HD, and D_2 molecules on graphite, primarily for electron energy of $\sim$62 eV, an energy at which low-energy-electron diffraction (LEED) can be used to detect ordered structures.[2] We first describe the experimental apparatus used for these measurements. We then show that the angular distribution is approximately isotropic for the scattering angles investigated (140°–170° from the normally incident electron beam). Time-of-flight (TOF) measurements show that the primary ions from monolayers are monatomic ions. The most energetic component of H^+ ions from H_2 has a threshold at electron energy near 30 eV, as expected for dissociative ionization such as occurs from the antibonding state of the singly ionized diatomic molecular ion. A comparison of measurements for the D_2 monolayers on bare graphite with those on Kr-plated graphite indicates a larger proportion of low-energy ions for the D_2 on Kr-plated graphite. Retarding energy measurements are then presented for H^+ from H_2, for D^+ from D_2 on bare and Kr-plated graphite, for H^+ from HD, and for D^+ from HD. The effective positive-ion cross sections for the three isotopes are estimated and some general conclusions are discussed. In a separate paper, we measure the total ESD removal rate for H_2 and HD for 62-eV electrons by using desorbed positive ions to measure the coverage remaining on the surface.[23]

II. APPARATUS

Figure 1 shows schematically the end of the electron drift tube (*A*), the beam profile device (*B*), sample holder (*C*–*F*), thermal radiation shield (*H*), grids (*J*), channel plates (*K*), and phosphor screen (*L*). The following sections discuss the electron beam and substrate, the ion detection, and the adsorbate coverage.

A. Electron beam and substrate

The long-focal-length electron gun was the same as used for previous LEED studies.[2,3,24–26] A tungsten filament with an extractor electrode was followed by a cylindrical einzel lens. The energy full width at half maximum (FWHM) of the beam measured by the electron beam measuring device (*B*) described below was less than 1 eV. The beam could be turned on and off via fast pulses from an electronic pulse generator that was capacitively coupled to the electron gun extractor electrode. Deflection plates on the electron gun determined the direction that the electrons exited from the drift tube (*A*). An electron beam profile measuring device (*B*) was mounted behind a hole in the radiation shield below the sample. The entire sample mount could be translated up to bring the device *B* in line with the electron beam for measurements. The device consisted of a metallic cylinder of 4-mm inner diameter by 19-mm length, with one end half covered by a semicircular metal plate connected to the cylinder and the other end closed. The incident beam current was measured to within 5% accuracy when the beam went fully into the cylinder. The difference between secondary electron emission from the metal plate and from the inside of the cylinder permitted

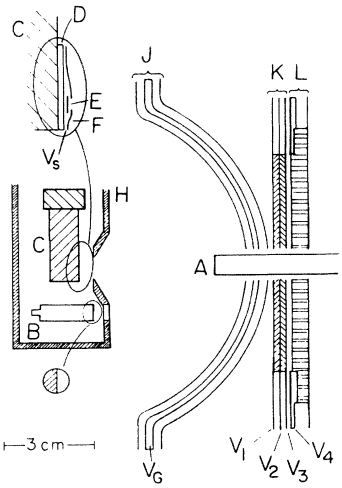

FIG. 1. Schematic showing sample and detector region of apparatus. See text for details.

measurement of the beam profile in the horizontal direction by translating the device across the beam.[27]

The graphite sample (*E*) used was extracted from calcite rock, cleaved in air, baked to about 800 °C in a separate vacuum, and then mounted in air on the sample holder. Previous Auger experiments[25] have shown that such surfaces have at most small traces of oxygen and nitrogen after bombardment by large electron fluxes. Measurements presented later in this paper provide further evidence for small amounts of trace impurities on this particular sample. In structural measurements using LEED such as in Refs. 2, 3, 24, and 25, there has always been good agreement with neutron diffraction and heat-capacity measurements on large area graphite surfaces. Thus it seems likely that the trace impurities are localized at steps or grain boundaries on the surface.

The sample was mounted on an electrically insulating thermal conductor (*D*) so the sample could be electrically biased via a copper plate (*F*) at potential V_S. The insulator *D* was a 0.75 mm thick sapphire crystal with an evaporated layer of germanium followed by an evaporated layer of gold on both sides with an indium layer between the copper cold finger and the back of the insulator. The metallic layers were intended to minimize any temperature jump at the interfaces between the copper cold finger *C* and the sapphire *D* and between the sapphire *D* and the graphite crystal *E*. The temperature of the cold finger *C* measured by a calibrated thermometer was typically 6 K for measurements with physisorbed H_2, HD, and D_2. Observation of the commensurate phase[1,2] of H_2 with LEED even when this thermometer indicated 16 K indicates that the graphite crystal is no more than 4 K warmer than the Cu block. The radiation shield (*H*) was electrically grounded and at a temperature below 20 K during normal operation.

For TOF ESD measurements the electron pulse width *W* was typically 0.15 μs, with a repetition rate of 50 kHz. In the on state, the voltage on the extractor electrode of the electron gun was +13 V with respect to the center of the tungsten filament; in the off state it was −2 V. For these pulse parameters and a typical $V_S = +8$ V bias applied to the sample, the average current for pulses of electrons of 63 eV energy relative to the sample was 0.5 nA. The spatial FWHM of the beam as measured by the beam profile device *B* in Fig. 1 was 1.1 mm, larger than used for previous LEED measurements.[2,3,24] This lowered the quality of LEED patterns used for coverage determination. The bias V_S on the sample could cause the width to be slightly different under measurement conditions. The spatial FWHM increased for electron energies below 40 eV to greater than 2 mm. Except for data used to estimate the effective positive-ion cross sections, the electron gun pulses were on continuously for the measurements described here. The sample bias V_S caused the positive ions to have an energy of at least eV_S (*e* is the magnitude of the elementary charge, contact potential corrections are not included), as they crossed the approximately 6-cm drift space from the grounded radiation shield *H* to the grounded first hemispherical grid *J*. A metal tube that provides an effusive source of gas blocks a small part of the drift space; its ion shadow can be seen in Fig. 2.

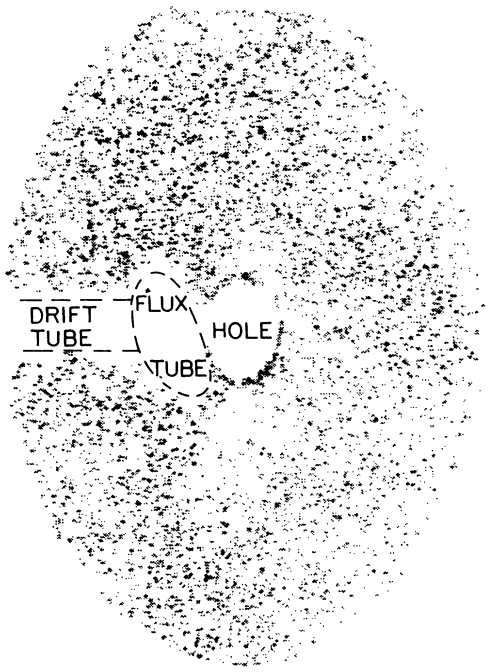

FIG. 2. Positive ion image from H_2 on graphite at 65 eV electron energy. The digital image was not corrected for the rectangular pixels of the CCD camera. The electron gun drift tube blocks part of the mirror used to observe the phosphor screen. An ion shadow is formed of the end of the gas flux tube. The central area is the hole in the channel plate and phosphor screen assembly. The image shown is the sum of four images of 1/25 s duration each. Sample bias was $V_S = 0$.

B. Ion detection

The second and third hemispherical grids were biased positively (V_G) for retarding energy analysis of the emitted ions. The bias applied to the front of the first channel plate was $V_1 = -2000$ V relative to the grounded fourth hemispherical grid, except for the data from H_2 in Fig. 2 and Fig. 3(a), where $V_1 = -700$ V. This bias helped to minimize differences in transit time between ions exiting the grids at different angles and to provide a good secondary electron yield for ions hitting the front of the first channel plate. Estimates of the efficiency of detecting H^+ ions hitting electron multipliers of similar composition vary from 0.40 to 0.85; the efficiency of detecting D^+ could be slightly smaller than that for H^+ (Ref. 28). For grid bias $V_G > 13\ \text{V} + V_S$, background counts in the time window used for ion detection ($0.8\ \mu\text{s} < t < 8\ \mu\text{s}$) were randomly distributed, ruling out any observable signal due to metastable neutrals.

A bias of $V_3 - V_2 = V_2 - V_1 = +1000$ V was usually used from front to back of each of the two channel plates *K*; the back of the first channel plate was electrically connected to the front of the second channel plate. A resistor ($R = 7\ \text{M}\Omega$) was placed between a 1–5 kV power supply and the phosphor screen *L*, biased at V_4; a capacitor ($C = 0.01\ \mu\text{F}$) coupled output current pulses from the phosphor screen to a fast preamp followed by a discriminator and pulse shaper. Tests with electrons uniformly

distributed across the 75-mm-diam channel plates showed that the effective dead time for such events was < 1 μs. The count rate at the discriminator output could be recorded as a function of time by a standard interface to a personal computer. The counting and sampling rates were varied depending on count rate and its rate of change with time.

In addition to recording the total counts, the discriminator output could be sent to a time-to-amplitude converter started by the pulse sent to the electron gun and typically set for 4 or 8 μs maximum time. The *average* number of detected ions per pulse was less than 0.6 for all TOF data, ensuring that events at later arrival times are accurately counted. TOF data were accumulated in a 512 channel multichannel analyzer for 20 s duration. The zero time reference for presenting the data is taken at the start of the earliest signal from photoelectrons ejected from the front of the channel plate by soft x rays produced when the primary electron beam strikes the sample. The main differences in our TOF detection system from one used for study of ESD of physisorbed D_2 from Pd(111) (Ref. 19) are that our hemispherical grids facilitate ion-energy analysis and that our phosphor screen allows visual observation (via a mirror[26]) of the ion angular distributions at the same time as the events are counted or sent to the TOF analyzer. Ion angular images were taken with a charge coupled device (CCD) camera using the computer system developed by Eden and Fain.[29] Due to spatial spreading between the back of the first channel plate and the front of the second channel plate, the secondary electrons created by ion impact on the front of the first channel plate occupy a wider spatial area on the phosphor screen than the 25 μm channel diameter.[30]

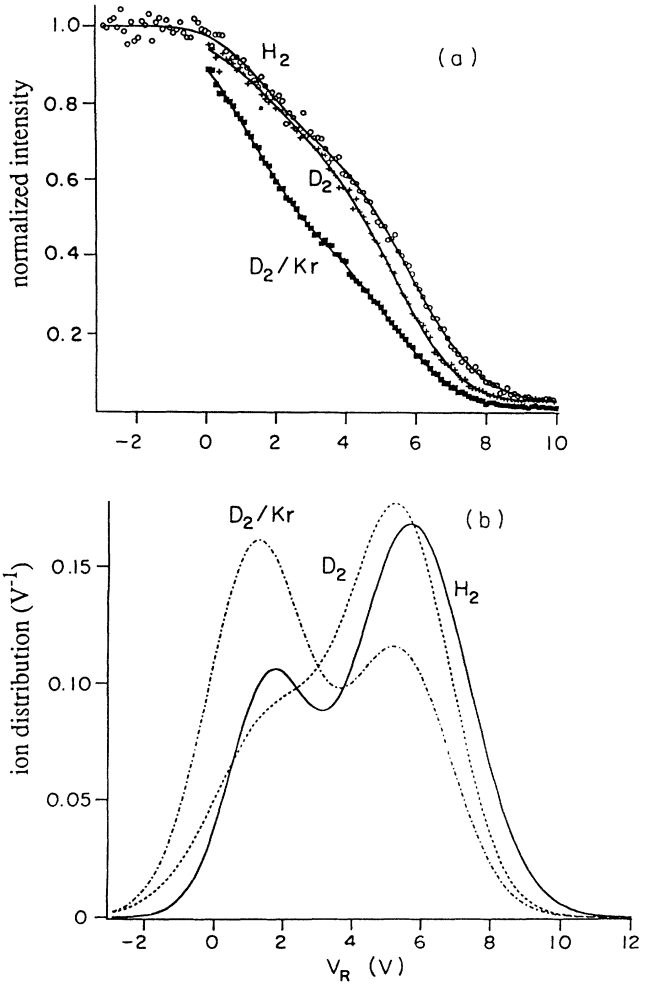

FIG. 3. Retarding potential measurements for H_2 and D_2. (a) Normalized ion count rate versus retarding potential $V_R = V_G - V_S$ for H_2 (open circles), D_2 on bare graphite (crosses), and D_2 on Kr-plated graphite (filled squares). The D_2 data are from the same conditions as the data in Fig. 6; the H_2 data are for a lower coverage than the D_2 data. (b) Energy distributions deduced from fits to data in (a), normalized to the same total area. The solid line is H_2; the dashed line is D_2 on bare graphite; the dash-dotted line is D_2 on Kr-plated graphite.

Deconvoluting these spectra to get energy distributions is difficult due to uncertainties in the total TOF drift distance and to the fact that the excitation pulse width W was a significant fraction of the ion flight time.[31] Energy distributions were obtained from measurements of the total ion count rate or of the count rate in a selected TOF time window as a function of applied potential difference $V_R = V_G - V_S$ between the retarding grids and the sample, with the potential V_G changed in small steps. The retarding field data were fit to the integral of one or two Gaussian peaks plus a constant background to determine the energy distribution, with a possible systematic error in the energy scale due to the unknown contact potential difference between the sample and the retarding grid.

C. Adsorbate coverage

The background pressure remote from the sample area was less than 4×10^{-10} torr before the gas flux was turned on; the background pressure in the vicinity of the sample was much lower due to cryopumping by the radiation shield H in Fig. 1. A steady-state coverage in the absence of the electron beam could be established by keeping a constant gas flux to the sample. The local pressure at the sample with the flux on is estimated to be $< 10^{-8}$ torr of H_2, HD, or D_2.

Measurements at room temperature with the fluxes used at low temperature revealed no detectable ion signal from the local pressure caused by the gas flux. As discussed previously,[24] coverage loss in the absence of the electron beam is believed to be due to desorption by infrared radiation from the room temperature LEED optics. For the TOF and retarding field measurements, measurements were taken under steady-state conditions where the total desorption by the electron beam produced a reduction in the surface coverage that was greatest at the center of the electron beam.[2,23] (The resulting ESD produced a larger surface coverage variation within the electron beam than for the LEED measurements for H_2, HD, and D_2 in which the electron beam was on for less than 1 s per image.[2,3,24]) In order to have uniform coverage for estimating the total effective cross section for positive ions in Sec. VI, the initial count rate

was measured in less than 1 s, after the flux had been on several minutes and the electron beam had been off.

For these experiments, surface coverages could be independently estimated by LEED in some cases. (a) For H_2, HD, and D_2 on graphite, the commensurate-incommensurate transition which occurs at 6.3×10^{14} molecules/cm^2 can be detected by a large decrease in intensity at 62-eV electron energy at the commensurate spot position with increasing coverage.[2] Previous experiments[2,3] showed that for the fluxes used in this experiment, the maximum surface density is a maximally compressed monolayer[1] of about 1×10^{15} molecules/cm^2. The crystal quality was not always sufficient to resolve the LEED patterns of coverages between these two limits. With the beam on at 62 eV the steady-state coverage is estimated to be about $8(\pm2)\times10^{14}$ molecules/cm^2. For the effective ion cross-section measurements in Sec. VI, the coverage was about one half this value. (b) For Kr on graphite,[26] the commensurate monolayer also occurs at 6.3×10^{14} atoms/cm^2; for the experiment described in Sec. IV C the exposure of the crystal to Kr at 40 K was four times the amount necessary for a commensurate layer, giving a Kr coverage estimated to be $2(\pm1)\times10^{15}$ atoms/cm^2. (c) For D_2 on Kr-plated graphite, no distinctive change in the LEED has yet been detected which can be correlated with coverage. The D_2 flux used for the data in Sec. IV C was the same for Kr-plated graphite as for bare graphite. The sticking coefficient and desorption rate need not be the same for the two substrates, so it is difficult to estimate the coverage of D_2 on Kr-plated graphite.

III. ANGULAR DISTRIBUTION OF POSITIVE IONS

Figure 2 shows an image (uncorrected for the rectangular CCD pixels) of the angular distribution of desorbed positive ions for H_2 adsorbed on graphite; images for HD and D_2 were similar, although the time to acquire such an image was longer due to lower count rate. The most important feature of this image is the approximate isotropy of the angular distribution for the angles investigated (approximately 140°–170° from the forward direction of the normally incident electron beam). Of course, a strongly peaked emission at scattering angles greater than 170° cannot be ruled out from these measurements.

As mentioned in the Introduction, no preferred orientation is expected for the molecular axis of the adsorbed molecules. Thus the angular distribution can be compared to that occurring in the gas phase. Measurements of the angular distribution of H^+ produced by electrons of energy near 60 eV impacting gas phase H_2 have been made for scattering angles up to 145°.[12,13] The maximum anisotropy occurs for higher-energy protons. Data for 8.6-eV protons have been fit to a theoretical form predicted for the variation in excitation cross section for the $^2\Sigma_u^+(2p\sigma)$ antibonding state of the singly ionized diatomic molecular ion;[12] extrapolation of the gas phase data to the larger angles measured here indicates at most a 20% variation for 8.6-eV protons over the 140°–170° region shown in Fig. 2. If all protons of energy greater than 1 eV are included, gas phase results indicate even smaller anisotropy.[13] Thus the absence of any appreciable variation in ion counts over the angles investigated is consistent with the gas phase results combined with the absence of a preferred orientation of the adsorbed molecules.[4]

IV. TIME-OF-FLIGHT RESULTS

A. TOF of H_2, HD, D_2 and trace impurities on graphite

TOF spectra from 1.0–2.5 μs are shown for H_2, HD, and D_2 layers in Fig. 4 for incident electrons of energy 62 eV. The spectra have been normalized to the largest peak; the relative heights are discussed below in Sec. VI on effective ion cross sections. The sample bias of $V_S=8$ V decreases the transit time of all ions, and affects the transit time of low-kinetic-energy ions the most. Since most of the drift path is field free, the time of arrival of a given ion will be given approximately by $t=d/\sqrt{2(eV_S+K)/m}$, where $d\sim6.6$ cm is the effective drift distance, K is the kinetic energy of the ion when emitted at the surface, and m is the ion mass. The H^+ ions emitted with near-zero K should arrive before D^+ ions with $K=8$ eV, permitting a separation of the H^+ and D^+ signals from HD. (A $V_S=+8$ V bias is also used for Figs. 5 and 6.) The ratio of times for the D^+ from D_2 peak to the H^+ from H_2 peak is $(1.90\pm0.03\ \mu s)/(1.33\pm0.04\ \mu s)=1.43\pm0.04$, close to the $\sqrt{2}$ value expected if the energy distributions were identical. The difference in H^+ arrival times from HD vs H_2 and in D^+ arrival times from HD vs D_2 is due to significant differences in ion energy distributions between the homonuclear and heteronuclear molecules. The lower number of D^+ relative to H^+ from HD, the energy differences of H^+ and D^+ from HD, and other details for each adsorbed isotope are discussed below.

The shoulder at the start of the signal from D_2 is due to H^+ from trace amounts of one or more impurities

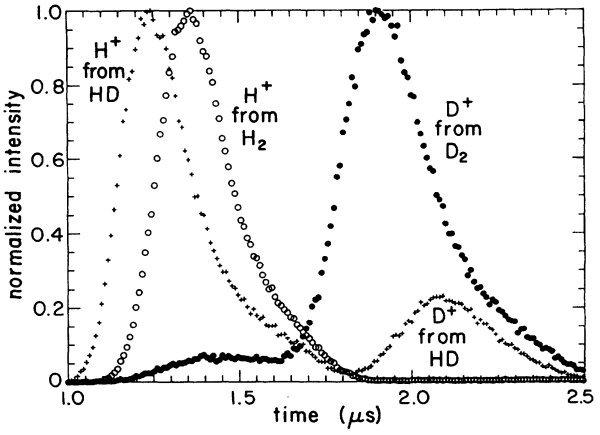

FIG. 4. TOF data for incident electron energy of 62 eV for coverage of approximately one monolayer for H_2 (open circles), D_2 (filled circles), and HD (plusses) on graphite at 7 K. The counts have been normalized to the largest peak. The sample potential is $V_S=8$ V, the retarding grid potential is $V_G=0$, and the electron pulse width is $W=0.15\ \mu s$.

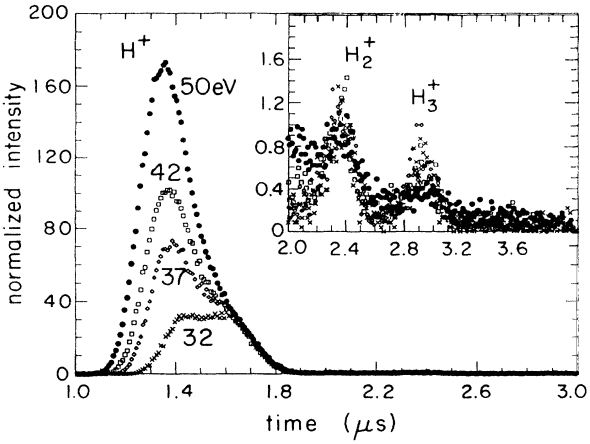

FIG. 5. TOF data H_2 on graphite for incident electron energies of 32 eV (crosses), 37 eV (open diamonds), 42 eV (open squares), and 50 eV (filled circles). The vertical scales were normalized by the incident electron current. $V_S=8$ V, $V_G=0$, $W=0.15$ μs.

present on this graphite substrate. The magnitude of this background ion signal is only slightly changed by large fluences of high-energy electrons that easily remove physisorbed H_2, HD, or D_2. The background is present at all temperatures. This signal is most noticeable in the D_2 measurements because D_2 has a lower ion yield than HD or H_2 and D^+ ions from D_2 occur at later times than most of the H^+ ions from the impurity. This signal at 1.2 μs $< t <$ 1.5 μs was slightly *less* for D_2 on graphite than for the bare graphite, indicating that the impurity was at least partially covered or displaced by the D_2. Thus the impurity signal cannot be subtracted away easily.

The TOF spectrum for the impurity was slightly different in different experiments; for $V_S=8$ V it was typically in the time region from 1.1 μs to 2.0 μs. For HD (H_2) under the conditions of Fig. 4, the signal at the main

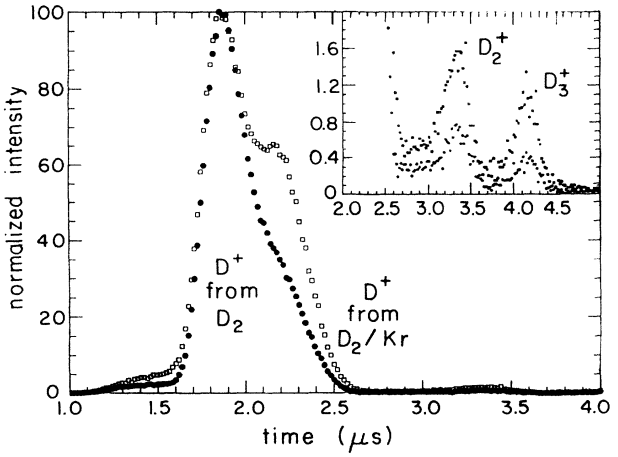

FIG. 6. TOF data for incident electron energies of 62 eV for D_2 on Kr-plated graphite (open squares) compared with D_2 on bare graphite (filled circles). The data have been normalized to the peak at 1.9 μs. $V_S=8$ V, $V_G=0$, $W=0.15$ μs.

peak was a factor of 10 (20) greater than the background on the bare crystal. The background signal is expected to arise after freshly cleaved graphite crystals are exposed to electrons at low temperatures, due to electron induced decomposition or dissociation of residual impurities which can adsorb at low temperatures. (As an extreme example, LEED studies of ethylene physisorbed at low temperatures showed a rapid irreversible degradation of the graphite substrate due to electron fluence.[29]) Much smaller peaks from the impurity could be observed at longer times: these peaks are tentatively assigned to OH^+ or O^+, CO^+, and $CO_2{}^+$. The trace impurities yielding these peaks may be correlated to the difficulty of obtaining good incommensurate LEED patterns from this crystal.

B. TOF of H_2 as a function of electron energy

TOF spectra for H_2 are shown in Fig. 5 for incident electron energies of 32, 37, 42, and 50 eV, approximately corrected for different electron currents. Two important features in Fig. 5 are similar to Stulen's results for physisorbed D_2 monolayers on Pd(111) saturated by chemisorbed D:[19] the diatomic and triatomic species are a small fraction of the monatomic species; the proportion of higher energy monatomic ions ($t < 1.6$ μs in this case) to the lower-energy monatomic ions ($t > 1.6$ μs in this case) increases significantly with electron energy above 30 eV. In Stulen's studies the triatomic peak was identified as the result of monatomic ions attaching to diatomic neutral molecules,[22] especially in the outer layers of a multilayer film. The triatomic peak and higher mass peaks from odd number of nuclei were observed to increase significantly as additional physisorbed layers were added on top of the first physisorbed monolayer. Thus an increase in the triatomic peak relative to monatomic peak at a given electron energy is an indicator of higher coverage.

Although the gas flux to the sample was kept constant, the effective coverage of H_2 in Fig. 5 is decreasing with increasing energy as the total removal by ESD (Ref. 23) reduces coverage more at higher electron energies. This reduction in coverage is due to the increasing total desorption caused by a probable increase in total effective desorption cross section and a definite increase in current density with increasing energy. (There may be some spillover of the electron beam onto the Cu sample holder at the lowest energy due to the spatial FWHM being greater than 2 mm. The electron-beam width decreases as the energy is increased.) The total ion signal from H_2 normalized by the incident electron current falls as the electron energy is increased from 50 to 100 eV. For HD, where Ref. 23 shows that the total ESD effect is smaller, the normalized ion signal does not fall until the electron energy exceeds 70 eV. Thus one cannot use data such as that in Fig. 5 to determine quantitatively the change in ion yields with electron-beam energy. The small change in normalized ion signal from the monatomic ions at the longer times ($t > 1.6$ μs in this case) and from the diatomics and triatomics could be due to the decreasing effective coverage counteracting an actual increase in ion yield as

the electron energy increases.

The incident electron energy where the higher-energy monatomic ions start to dominate the spectra is close to the 28-eV threshold for dissociative ionization from the $^2\Sigma_u^+(2p\sigma)$ antibonding state of the diatomic positive ion.[12,13,19] Thus the higher-energy monatomic ions at 62 eV are expected to arise from that state. Lower-energy ions are expected to arise from autoionizing states.[11,14]

C. TOF of D_2 on bare versus Kr-plated graphite

For a surface with readily available electrons such as graphite or the previously studied Pd(111) saturated with D,[19] the excited molecular states produced by electrons can be deexcited ("quenching" the ion emission) by interaction with free electrons from the substrate. The deexcitation rate is expected to be lower on an insulator surface. A first approximation to an insulator surface was studied by adsorbing a coverage of Kr on the graphite surface estimated to be $2\pm1\times10^{15}$ atoms/cm^2 and then comparing the signal from D_2 on this surface with the signal from D_2 on bare graphite. (The D_2 flux on the surface was almost the same for bare and Kr-plated graphite. Coverage on the Kr-plated surface could be higher; it could not be directly measured.) The result is shown in Fig. 6. The relative increase in the low-energy D^+ ($2.1\ \mu s < t < 2.4\ \mu s$) for D_2 on Kr-plated graphite is most likely caused by decreased quenching of the pathways leading to lower-energy ions. (A reduced image charge force resulting from the Kr layer could in principle lead to more low-energy ions escaping. By itself, such a reduced image force would be expected to increase the most probable ion energy; as seen in the data in the next section, there is no detectable change in the most probable energy of the faster ions.) A similar increase in the proportion of low-energy monatomic ions was observed as the coverage was increased above a monolayer for physisorbed D_2 on Pd(111) saturated with D.[19] In that situation an increase in the low-energy component can also arise from inelastic scattering by the outer layers of higher-energy ions emitted closer to the surface. The increased proportion of diatomic and triatomic ions may also be caused by reduced quenching or it may be due to higher D_2 coverage on the Kr layer.

V. RETARDING FIELD ANALYSIS RESULTS

In order to compare the ion energies with results from the gas phase,[12,13] retarding field analysis (RFA) was done by measuring the positive-ion count rate as a function of bias V_G on the retarding grids.

A. RFA for H_2 and D_2

The normalized positive-ion intensity versus retarding voltage $V_R = V_G - V_S$ is shown in Fig. 3(a) for H_2 and D_2 layers for $V_S = +8$ V. The data in Fig. 3(a) were fit to a constant background term plus the integral of two Gaussian peaks of adjustable height, position and width; the fits are shown by solid lines. (Fits to polynomials gave similar results; the quality of the data did not justify more than the seven adjustable parameters for the two-Gaussian-peak fit.) Figure 3(b) shows the sum of the two peaks for the three fits, normalized to the same total area. If there were no contact potential correction, Fig. 3(b) would be the distribution in ion kinetic energy K. Table I shows the important parameters for the two peaks resulting from these fits. The small differences between the peak energies for H^+ from H_2 and D^+ from D_2 on bare graphite are consistent with the quantitative comparison of the TOF peak positions noted earlier. Gas phase results for the energy distributions of H^+ from H_2 and D^+ from D_2 show small differences between H_2 and D_2.[14,15] However, details such as the location of peaks in the energy distributions from either element vary with angle of observation, incident electron energy, and apparatus used.[15] The large change at low energies for the D^+ from D_2 on bare and on Kr-plated graphite is qualitatively consistent with changes in the TOF spectra noted earlier.

Measurements of the area of the H_3^+ peak from H_2 as a function of the retarding voltage V_R indicate a drop in counts between 0 and +1 V and a most probable H_3^+ ion energy of about 0.5 ± 0.3 eV. An upper limit on the most probable energy of the H_2^+ peak is +1 eV; the background from the H^+ peak was much larger near the H_2^+ peak.

B. RFA using TOF signals from HD

Figure 7 shows TOF spectra for electrons of energy 62 eV incident on two HD coverages. Compared with the TOF data in Fig. 4, the pulse width has been shortened to $W = 0.05\ \mu s$ and the sample bias V_S increased to +12 V to better separate the H^+ and D^+ signals. Low-energy shoulders (at longer times) are evident on the H^+ peaks, especially at the higher coverage; these will be discussed below. The increase in size of mass 3, 4, and 5 relative to masses 1 and 2 at higher coverage may indicate that the

TABLE I. Parameters from fits to retarding field data for different ions, adsorbates (ads), and coverage (cov).

Ion;ads;cov	Position 1	FWHM 1	Position 2	FWHM 2	Area 2/total
$H^+;H_2$	1.6±0.1 eV	2.7±0.2 eV	5.7±0.1 eV	3.9±0.1 eV	0.71±0.02
$D^+;D_2$	1.8±0.4 eV	4.0±1.6 eV	5.4±0.3 eV	3.4±0.3 eV	0.63±0.13
$D^+;D_2$/Kr	1.2±0.1 eV	3.5±0.3 eV	5.3±0.1 eV	3.5±0.2 eV	0.43±0.04
H^+;HD;lo	2.7±0.4 eV	5.9±0.5 eV	7.8±0.1 eV	4.6±0.2 eV	0.64±0.05
H^+;HD;hi	2.5±0.2 eV	5.5±0.4 eV	8.0±0.1 eV	4.5±0.2 eV	0.60±0.04
D^+;HD;lo			2.59±0.02 eV	3.32±0.05 eV	1.0
D^+;HD;hi			2.66±0.02 eV	3.47±0.06 eV	1.0

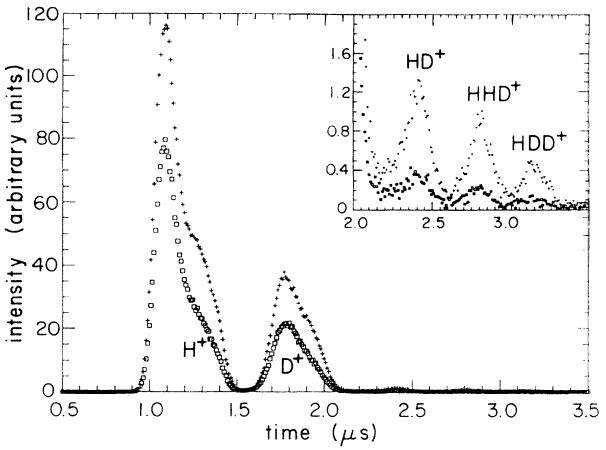

FIG. 7. TOF data for two coverages of HD on graphite at 60-eV electron energy. $V_G=0$, $V_S=12$ V, and $W=0.05$ μs. The higher coverage (pluses) is incommensurate and perhaps a partial bilayer; the lower coverage (open squares) is commensurate.

higher coverage is a partial bilayer.

For Fig. 8(a), the ion counts in spectra like those of Fig. 7 between 0.9 and 1.55 μs are taken to be H^+ and the counts between 1.55 and 2.2 μs to be D^+. Figure 8(a) shows the number of H^+ and D^+ as a function of the applied potential difference $V_R=V_G-V_S$. The data for H^+ in Fig. 8(a) were fit with the integral of two peaks, as for the retarding data for H_2 and D_2 discussed earlier; the data for D^+ were fit best by one peak. Figure 8(b) shows the energy distribution deduced; the sum of the H^+ and D^+ areas for low coverage is set equal to the sum for high coverage. Table I includes the parameters resulting from these fits. The most probable energies are 7.9 eV for H^+ and 2.6 eV for D^+ from HD. (A preliminary analysis of TOF data for sample bias $V_S=+8$ V and grid bias $V_G=8$ V gives somewhat higher most probable energies: 8.5 eV for H^+ and 3.4 eV for D^+ from HD, not including any contact potential correction.[31]) The difference in low energy cutoffs shown in Fig. 8(b) for the D^+ ions compared to the H^+ ions may be an artifact caused by the lowest-energy H^+ ions being slowed to $t>1.55$ μs for 1 V$>V_R>-2$ V. An increase in the ions counted as D^+ seen in the higher coverage D^+ data in Fig. 8(a) could be a result of this artifact; the fitting procedure ignores this unphysical increase for D^+, but will include the artificial decrease for H^+.

If quenching of the excited states is dominated by electrons from the graphite, the energy distributions could change as the adsorption sites change from the commensurate sites at the lower coverage to the wide variety of sites for the incommensurate, higher coverage. In addition the average distance of molecules from graphite is expected to increase from 2.82 Å for a commensurate HD monolayer to 2.95 Å for an incommensurate HD monolayer.[32] The changes seen in Fig. 8(b) are rather small, with a slight increase in the proportion of low-energy ions for the higher coverage H^+ energy distributions. This may be due to a partial bilayer causing an increase in low-energy ions as seen for D_2 on Kr-plated graphite. There is a small change in the ratio of the number of H^+ to the number of D^+ as the coverage is increased, from 3.1 to 2.9 if one counts all ions detected when $V_R=-4$ V. (A preliminary analysis of TOF data for sample bias $V_S=+8$ V and grid bias $V_G=8$ V gives a somewhat higher value: 3.5 for 61 eV incident electron energy and lower values for lower energies.[31])

For gas phase HD the energy of H^+ ions is twice that of D^+ ions due to momentum conservation.[14] About 1.6 times as many H^+ as D^+ are detected at an angle of 90° to the incident 50 or 100 eV electrons.[14] Some differences between the gas phase and ESD ratios of H^+ to D^+ can be due to the different angle of detection relative to the

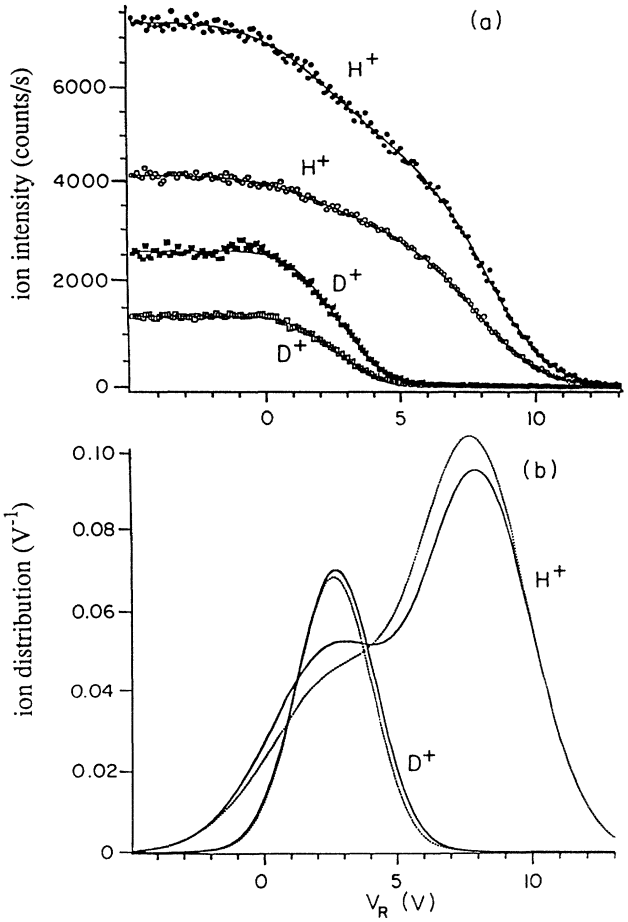

FIG. 8. Retarding potential measurements for HD: (a) Count rate in the H^+ and D^+ peaks from HD as a function of the applied retarding potential $V_R=V_G-V_S$ for $V_S=12$ V and $W=0.05$ μs, as in Fig. 7. The upper two curves are H^+ counts: filled circles (high coverage), open circles (low coverage). The lower two curves are D^+ counts: filled squares (high coverage), open squares (low coverage). The ratio of the number of H^+ to the number of D^+ changes slightly, from 3.1 to 2.9 for $V_R=-4$ V. (b) Energy distribution curves for H^+ (curves with main peak at 7.9 eV) and D^+ from HD (curves peaked at 2.6 eV) as a function of the applied retarding potential (V_G-V_S) for $V_S=12$ V and $W=0.05$ μs calculated from the fits to the data of Fig. 8(a). The curves are normalized to give the same total area of H^+ plus D^+ at the two coverages. At the higher coverage (solid lines) there is a slightly larger proportion of low-energy H^+ ions than at the lower coverage (dashed lines).

incident beam: 140°–170° in the ESD experiment vs 90° for the gas phase data.[14] The 90° angle was chosen in the gas phase measurement to suppress the contribution from the antibonding HD^+ state; the data for H_2 in the same experiment were fitted with contributions from various autoionizing states. Possible reasons for the differences from the gas phase are discussed in the conclusions section.

VI. EFFECTIVE ION CROSS SECTIONS FOR H_2, HD, AND D_2 ON GRAPHITE

For the case of uniform coverage, the number of detected ions P is $P=P_b+\gamma\sigma_p I\theta$, where P_b is the background ion signal, θ is the coverage in molecules per unit area, I is the number of electrons per second, σ_p is the total effective cross section for producing positive ions that escape the surface, and γ is the efficiency of detection, which can depend on the ion mass and energy distribution. For calculating the total effective positive-ion cross section, the initial counts when the electron beam is first turned on is used to ensure that the coverage is constant inside the region probed by the electrons. For measuring the effective ion cross sections, coverages less than the commensurate monolayer value were used. Uncertainties in the surface coverage between the different adsorbates create approximately ±40% uncertainty in the relative effective ion cross sections. Assumptions made in estimating the detection efficiency were: 30% of the emitted ions enter the detection range of 140°–170°; 50% of the ions are not detected due to scattering by the four grids; and 70% of the H^+ and D^+ ions hitting the channel plate[28] are detected for $V_1=-2000$ V. These assumptions give $\gamma=0.10$, with an estimated uncertainty of a factor of 2. This gives total effective positive-ion cross sections within a factor of 2 for $V_S=8$ V and $V_G=0$ V of 1×10^{-5}, 3×10^{-6}, and 1×10^{-6} nm^2 for H_2, HD, and D_2. The isotope dependence of the total effective ion cross sections is qualitatively consistent with the dominant dependence expected for deexcitation of ions of comparable energies by tunneling through a barrier[8]: $\exp(-c\sqrt{M})$. A conclusive test of this predicted mass dependence requires more accurate measurements of the relative yields.

The monatomic ion cross section in the gas phase at 60 eV is about 1×10^{-3} nm^2.[18] Roughly a factor of 10^2 (10^3) *less* monatomic ions per electron are produced at 62 eV from H_2 (D_2) physisorbed on graphite compared to the gas phase. The major difference between the results we measure for the different isotopes is probably due to different quenching effects due to electrons from the graphite substrate. For example, consider the monatomic ions resulting from the dissociative ionization from the $^2\Sigma_u^+(2p\sigma)$ antibonding state of the diatomic positive ion. The relative velocity of the nuclei during the dissociation depends on the square root of the relative mass; the heavier nuclei take longer to separate, allowing more time for an electron from the substrate to tunnel to the diatomic positive ion.

The number of diatomic ions is approximately a factor of 100 smaller than the number of monatomic ions, giving effective ion cross sections of 1×10^{-7}, 3×10^{-8}, and 1×10^{-8} nm^2 for H_2, HD, and D_2. In the gas phase most of the ionization produces H_2^+ ions; the total ionization cross section[18] is the same for H_2 and D_2: about 1×10^{-2} nm^2 at 62 eV. Thus the effective diatomic ion cross sections for these monolayers on graphite are 10^{-5} to 10^{-6} smaller than for the gas phase. This is probably a result of the large quenching effects for the diatomic ions due to their lower kinetic energies and larger masses.

VII. CONCLUSIONS

Some of the results found here are similar to the gas phase: (1) the lack of a strong variation in angular distribution over the range investigated, (2) the increase in higher-energy monatomic ions as the electron energy is increased above 30 eV, and (3) the similarity in energy distributions for H^+ from H_2 to that of D^+ from D_2 (when both are on bare graphite).

Other results indicate clear differences from the gas phase: (4) the number of diatomic ions is a factor of 100 less than the number of monatomic ions compared to a factor of 10 more in the gas phase, (5) the effective ion cross section for H^+ from H_2 is a factor of 10 larger than that for D^+ from D_2, (6) the most probable energy of H^+ from HD is greater than twice the most probable energy of D^+ from HD, and (7) the number of H^+ from HD is three times greater than the number of D^+ from HD.

Other results have no analogy with the gas phase: (8) the change in energy distribution for D^+ from D_2 in going from bare to KR-plated graphite and (9) small changes in energy distribution with surface coverage.

In trying to understand the qualitative features operative for the monatomic ion production, some general ideas must be taken into account.

(a) *Changes in wave function at the surface.* Although the ground state of the physisorbed molecule is essentially an unhindered rotor, the wave functions and energies of the excited states involved in ion production can be different from the free molecule due to the presence of the substrate. For example, autoionizing states involve two excited electrons and may have a sufficiently greater spatial extent than the ground state to be changed by the substrate; thus their excitation rates can differ from those for a free molecule.

(b) *Recoil effects.* When an excited state such as $^2\Sigma_u^+(2p\sigma)$ antibonding state of the diatomic positive ion evolves with time, the fragment of the state going towards the ion detector is still strongly interacting with the fragment of the state going toward the substrate when the latter encounters repulsive forces due to the substrate. Thus recoil from the substrate during the decay process can change the energy of the detected ion.

(c) *Quenching of excited states.* The lifetime of the excited states can change due to interaction with the substrate in more complicated ways than just simple neutralization processes involved in scattering of monatomic ions.[20] The quenching rate will be stronger for excited states of greater spatial extent, for states that spend more time in the vicinity of the surface, and for surfaces with available electrons.

(d) *Image charge effects.* Although it is known that a simple image force effect is not appropriate for ions at these distances,[21] there is certainly a rearrangement of the substrate electrons due to the excited states near the surface that can affect the excited state wave functions and the resulting ion energies.

The much lower ion yield of D^+ from D_2 compared to that of H^+ from H_2 (item 5) was explained above as due to greater quenching of the excited states [item (c)] of D_2. Different quenching for different pathways producing monatomic ions could in general make the energy distribution for D^+ from D_2 different from that for H^+ from H_2.

The changes in the energy distribution for D^+ from D_2 on Kr-plated graphite compared to bare graphite (item 8) was also explained above as due to greater quenching of the excited states (item c). Due to the larger size of Kr atoms compared to carbon atoms in graphite, the physisorbed molecule will be further away from the Kr surface, which could also affect the effective excitation cross sections for autoionizing states that produce more low-energy ions [item (a)]. Finally the recoil effects (item b) can certainly be different because the Kr surface will not be as rigid as the graphite surface. If the recoil effect decreases the energy of the ions, it may be just enough to counteract an increase in energy expected for a decrease in image force [item (d)], explaining the absence of a change in the most probable energy of the faster ions.

Given the role of these factors for the heteronuclear molecules, one should not be surprised that the energy ratios (item 6) and number ratios (item 7) for H^+ to D^+ from HD are so different from the gas phase. The energy ratios (item 6) can be explained by naive image charge arguments [item (d)] plus contact potential correction if both kinetic energies are shifted by 2.7 eV; this seems unreasonably large. In the extreme example of recoil [item (b)] in which the nucleus going toward the detector takes all the internal energy, the ratio of energies will become 1, giving an effect in the opposite direction to the observed one.

The effect of the deexcitation [item (c)] on the number ratio (item 7) suggests that more deexcitation occurs when the deuteron end of the molecule is going toward the detector, which is consistent with overlap of the evolving state occurring sooner for this orientation due to the greater velocity of the proton end. This selective quenching could be different from the more energetic ions produced through the antibonding HD^+ state than for ions produced through autoionizing states. A more complete theory is needed to consistently explain the entire set of results we have presented here.

ACKNOWLEDGMENTS

We thank the following people: W. Liu for preliminary quantitative estimates of ESD removal rate for these adsorbates; R. Stulen for sending us a copy of his paper; A. Johnson for stimulating us to look at the positive ions desorbed and for many discussions; P. Williams for continuing assistance with the electronics; A. Johnson, P. Williams, J. Stoltenberg, M. Olmstead, E. Stuve, and W. Dougherty for lending us equipment essential for these measurements; R. Sandwith for help with interfacing the computer directly to the discriminator output; R. Storem for helping characterize the impurities; Z. Gortel, T. Madey, M. Olmstead, O. Vilches, R. Diehl, D. Hamann, T. Orlando, and L. Sorensen for useful discussions. This work was supported by NSF Grant No. DMR-91-19701.

*Author to whom all correspondence should be addressed. Electronic address: fain@phys.washington.edu

†Present address: Harvard University Science Center, 1 Oxford Street, Cambridge, MA 02138.

[1]H. Wiechert, Physica B **169**, 144 (1991).

[2]J. Cui and S. C. Fain, Jr., Phys. Rev. B **39**, 8628 (1989); J. Cui, S. C. Fain, Jr., H. Freimuth, H. Wiechert, H. P. Schildberg, and H. L. Lauter, Phys. Rev. Lett. **60**, 1848 (1988); **60**, 2704(E) (1988).

[3]W. Liu and S. C. Fain, Jr., Phys. Rev. B **47**, 15 965 (1993).

[4]A. D. Novaco and J. P. Wroblewski, Phys. Rev. B **39**, 11 364 (1989).

[5]R. E. Palmer and R. F. Willis, Surf. Sci. **179**, L1 (1987).

[6]P. R. Kubik, W. N. Hardy, and H. Glattli, Can. J. Phys. **63**, 605 (1985).

[7]H. J. Lauter, in *Phonons 89,* edited by S. Hunklinger, W. Ludwig, and G. Weiss (World Scientific, Singapore, 1990), p. 871.

[8]R. D. Ramsier and J. T. Yates, Jr., Surf. Sci. Rep. **12**, 243 (1991).

[9]H. S. W. Massey, in *Electronic Collisions with Molecules and Photo-ionization,* edited by H. S. W. Massey, E. H. S. Burhop, and H. B. Gilbody, Electronic and Ionic Impact Phenomena Vol. II (Clarendon, Oxford, 1969), p. 883 (threshold energies), p. 932 (ion-pair production).

[10]H. Tawara, Y. Itikawa, H. Nishimure, and M. Yoshino, J. Phys. Chem. Ref. Data **19**, 6179 (1990).

[11]M. Landau, R. I. Hall, and F. Pichou, J. Phys. B **14**, 1509 (1981).

[12]G. H. Dunn and L. J. Kieffer, Phys. Rev. **132**, 2109 (1963).

[13]J. J. Johnson and J. L. Franklin, Int. J. Mass Spectrom. **33**, 393 (1980).

[14]M. D. Burrows, L. C. McIntyre, Jr., S. R. Ryan, and W. E. Lamb, Jr., Phys. Rev. A **21**, 1841 (1980).

[15]G. Arena, V. Berardi, N. Spinelli, R. Velotta, and M. Armenante, Int. J. Mass Spectrom. **127**, 57 (1993).

[16]D. Rapp, T. E. Sharp, and D. D. Briglia, Phys. Rev. Lett. **14**, 533 (1965). These authors found the cross section for H^- production from H_2 for electron energies from 7 to 18 eV to be less than 2×10^{-6} nm^2; this is the most recent data given in a recent review of cross section measurements in Ref. 10.

[17]A. K. Edwards, R. M. Wood, A. S. Beard, and R. L. Ezell, Phys. Rev. A **37**, 3697 (1988). These authors found a ratio of double ionization to single ionization less than 10^{-3} from 0.4 to 1.9 keV; this ratio at 60 eV implies double ionization cross section less than 10^{-5} nm^2.

[18]D. Rapp, P. Englander-Golden, and D. D. Briglia, J. Chem. Phys. **42**, 4081 (1965). In the gas phase, the cross section for

producing monatomic ions of energy greater than 2.5 eV was found to be the same for H_2 and D_2: 5×10^{-4} nm^2 at 60 eV. The number of monatomic ions of energy less than 2.5 eV is estimated to be similar to that above 2.5 eV (see Ref. 15); this gives 1×10^{-3} nm^2 at 60 eV as an estimate for the monatomic ion cross section in the gas phase.

[19]R. H. Stulen, in *Desorption Induced by Electronic Transitions: Diet III,* edited by R. H. Stulen and M. L. Knotek (Springer-Verlag, Berlin, 1988), p. 39.

[20]H. Niehus, W. Heiland, and E. Taglauer, Surf. Sci. Rep. **17**, 213 (1993).

[21]P. Avouris, Annu. Rev. Phys. Chem. **40**, 173 (1989).

[22]T. M. Miller, J. T. Moseley, D. W. Martin, and E. W. McDaniel, Phys. Rev. **173**, 115 (1968).

[23]B. Xia and S. C. Fain, Jr., following paper, Phys. Rev. B **50**, 14 576 (1994).

[24]W. Liu and S. C. Fain, Jr., J. Vac. Sci. Technol. A **10**, 2231 (1992).

[25]R. D. Diehl and S. C. Fain, Jr., Surf. Sci. **125**, 116 (1983).

[26]M. D. Chinn and S. C. Fain, Jr., J. Vac. Sci. Technol. **14**, 314 (1977).

[27]M. G. Lagally and J. A. Martin, Rev. Sci. Instrum. **54**, 1273 (1983).

[28]J. P. Macau, J. Jamar, and S. Gardier, IEEE Trans. Nucl. Sci. **NS23**, 2049 (1976); R. A. Baragiola, E. V. Alonso, J. Ferron, and A. Oliva-Florio, Surf. Sci. **90**, 240 (1979).

[29]V. L. Eden and S. C. Fain, Jr., Phys. Rev. B **43**, 10 697 (1991).

[30]J. L. Wiza, Nucl. Instrum. Methods **162**, 587 (1979).

[31]B. Xia and S. C. Fain, Jr. (unpublished).

[32]A. D. Novaco (private communication).